Supporting information for:

Magnetostaltic pumping in an ex vivo Extracorporeal Membrane Oxygenation model

MohammadReza Zolala[1], Veronique Heim[2], Cécile V. Denis[3,4], Peter J. Lenting[3], Pierre H. Mangin[2], Thomas M. Hermans[1,5]*

[1]Université de Strasbourg, UMR7140, Strasbourg, France. [2]INSERM, EFS Grand-Est, BPPS UMR-S1255, FMTS, Strasbourg, France. [3]Université Paris-Saclay, INSERM, Hémostase Inflammation Thrombose HITh U1176, 94276, Le Kremlin-Bicêtre, France. [4]Centre Hospitalier Régional Universitaire de Nancy, 54000 Nancy, France. [5]IMDEA Nanociencia, C/ Faraday 9, 28049 Madrid, Spain.

*e-mail: Thomas.Hermans@imdea.org

Contents

1. Chamber optimization

A chamber moves the fluid inside the magnetic pumps, and the design of the chamber had to meet some specific characteristics, such as the ability to move the blood from the inlet to the outlet and to constantly rotate the ferrofluid in the circuit (Fig. S1a). At the end of the path, the ferrofluid from the embedded nozzle returns to the beginning of the circuit, and the blood is forced out of the outlet nozzle (Fig. S1b). On the other hand, the blood inflow must have the necessary space to enter the chamber so that it does not constrict and stop. For this purpose, the paths of ferrofluid and blood are separated by a distance of 5 cm from the beginning of the chamber (Fig. S1c). This separation ensures that the ferrofluid does not block the blood inflow and that the blood always flows at the beginning of the path. In addition, the chamber should be able to circulate the ferrofluid and prevent it from leaving the chamber. In particular, at the end of the cycle, in the area where the fluid exits the tube into the large part of the chamber, the fluid quickly enters a larger area. Due to the surface change in this area of the chamber and the pressure caused by the liquid, part of the ferrofluid rises with the liquid to the outlet nozzle (Fig. S1d). To eliminate this phenomenon, a baffle was installed at the liquid outlet where the surface of the chamber rises, so that the ferrofluid cannot easily reach the upper part of the chamber (Fig. S1e). In other words, at the end of the cycle, there is a competition between the force of the rotating magnets and the pressure force resulting from the flowing mass to change the direction of the ferrofluid particles. Basically, the design should be such that at the end of the path, the magnetic force can overcome the flow force so that the ferrofluid remains in circulation.

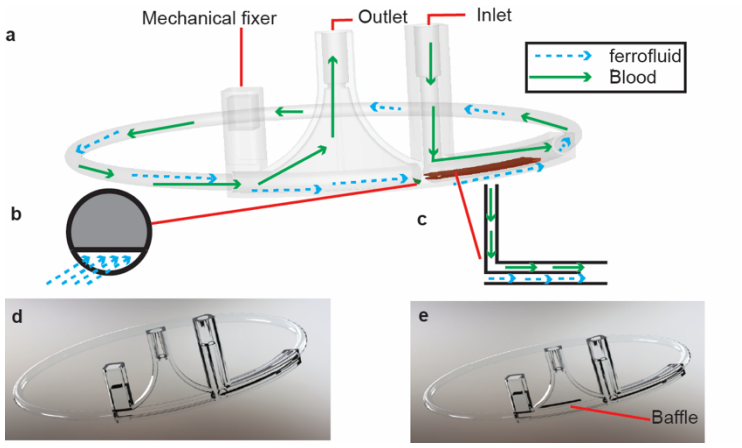

Fig. S1 | a, Structure of the chamber with outlet and inlet nozzles and return of ferrofluid to the initial circuit. **b,** Cross-section of ferrofluid return at the beginning of the cycle. **c,** The movement of ferrofluid and blood at the beginning of the cycle and the inlet nozzle. **d,** The chamber is designed without the baffle. **e,** The chamber is designed with the baffle.

In addition to installing the baffle inside the chamber, structural changes were made outside the chamber and to the body of the pump. For example, two magnets were also removed from the fixed disk (Fig. S2a,b). At the end of the pathway, the difference in magnetic properties between ferrofluid particles and blood is exploited. For this purpose, two fixed magnets were removed from the fixed disk at the end of the pathway, increasing the time required to apply the magnetic force to the ferrofluid particles at the end of the cycle (Fig. S3a,b).

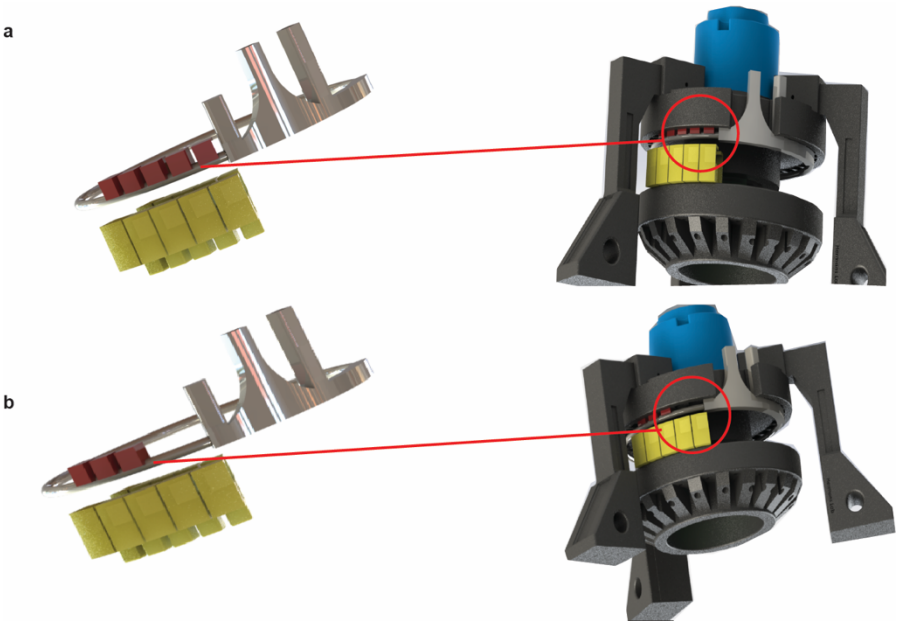

Fig. S2 | a, Fixed disc with all magnets **b,** Removed two magnets at the end of the cycle.

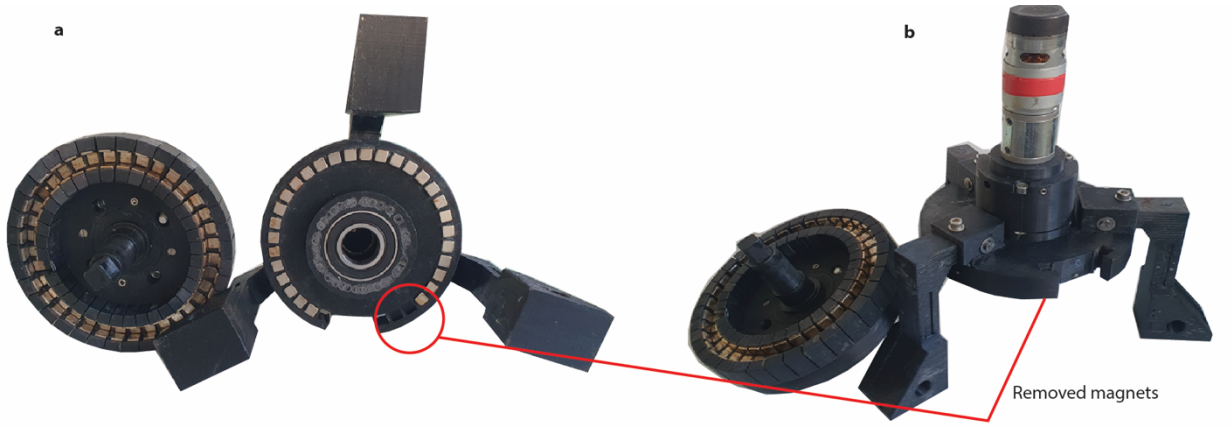

Fig. S3 | The position of two remote magnets in two different pump positions. **a,** The front view of the fixed disc. **b,** The stationary view of the pump.

To see the results of these two ideas and designs, the magnetic pump (**QR2**) was tested with distilled water and ferrofluid. At the start of each experiment air was removed from the setup and the flow was allowed to stabilize for 3 minutes. After this the distilled water was recirculated through the pump for 20 minutes before being collected. The total iron concentration is shown in Fig. S4. It was found that the use of the baffle with the simultaneous removal of two magnets at the pump outlet has a great effect on maintaining the circulation of the ferrofluid (see "Baffle + remove 2 magnet", black line; note: lowered leached Fe concentrations are preferable).

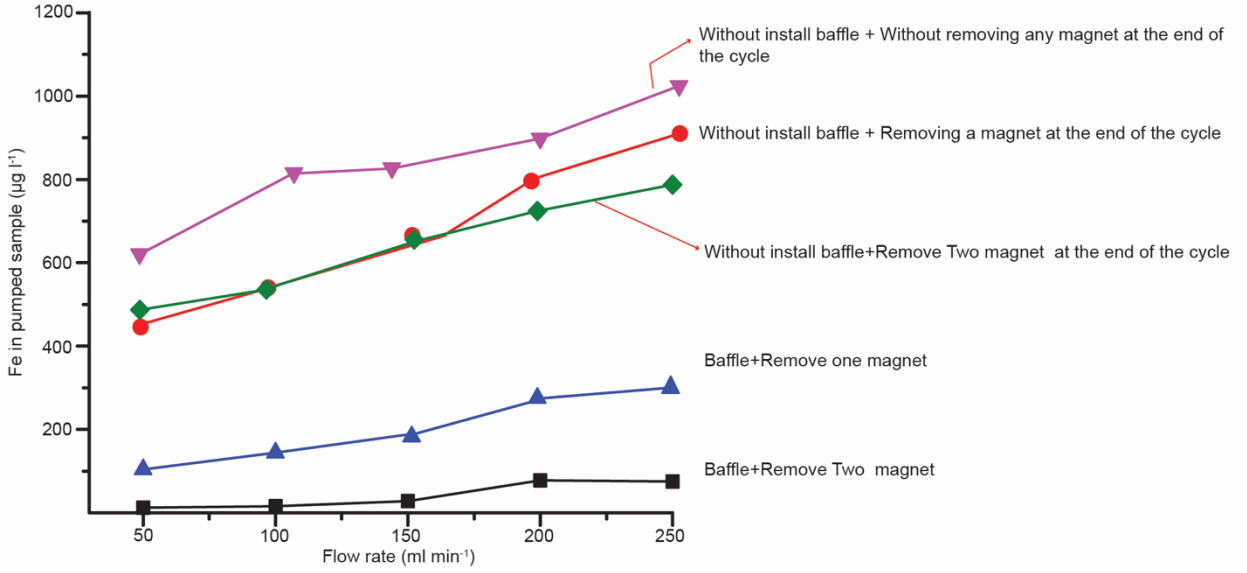

Fig. S4 | The effect of the presence of baffles and removal of the magnets on the ferrofluid separation in the chamber (and therefore also the leaching).

This chambers for each of the rotary magnetostaltic pumps were 3D printed as show in Fig. S5 below.

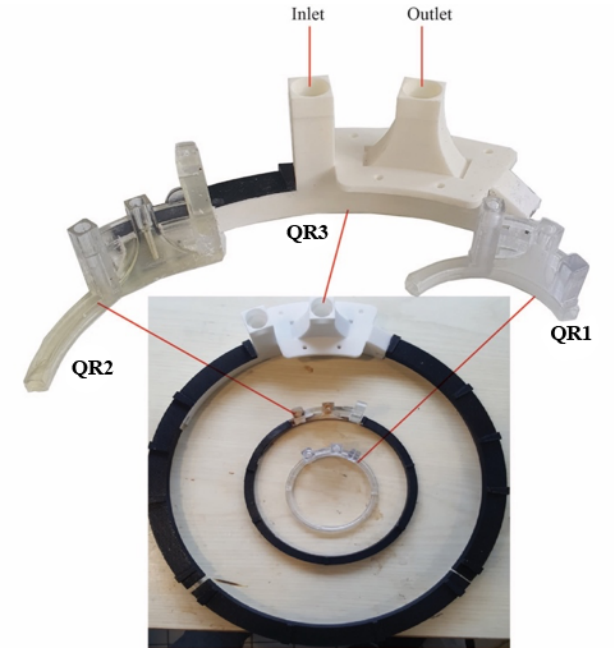

Fig. S5 | QR3, **QR2** and **QR1** pump chambers printed with a 3D printer. **QR3**, **QR2** and **QR1** pump chambers printed with a 3D printer. The 3D printed part for each pump was connected to silicone tubing: for a **QR1** tube that is 20 cm long, 3.2 mm in external diameter, and 2 mm in internal diameter. For a **QR2** tube that is 35 cm long, 8 mm in external diameter, and 5 mm in internal diameter. For a **QR3** tube that is 80 cm long, 12 mm in external diameter, and 9.5 mm in internal diameter.

2. Linear pump (QL)

2.1 Materials and manufacturing methods

Due to the structural conditions of the shafts, it was not possible to manufacture them using standard Computer Numerical Control (CNC) machining, considering that the shaft diameter is 15 mm and the depth of each cube magnet is 10 mm (Fig. S6 and Fig. S7a), thus leaving only 5 mm thickness. For this reason, 3D printing using stainless steel grade 316 was used. By applying a point force of approximately 500 N on the shaft and comparing ABS polymer and reinforced stainless-steel grade 316, it is possible to simulate the amount of deformation of the shaft in the magnetic field (Fig. S6). This confirmed that ABS was not sufficiently strong and stainless steel was absolutely required.

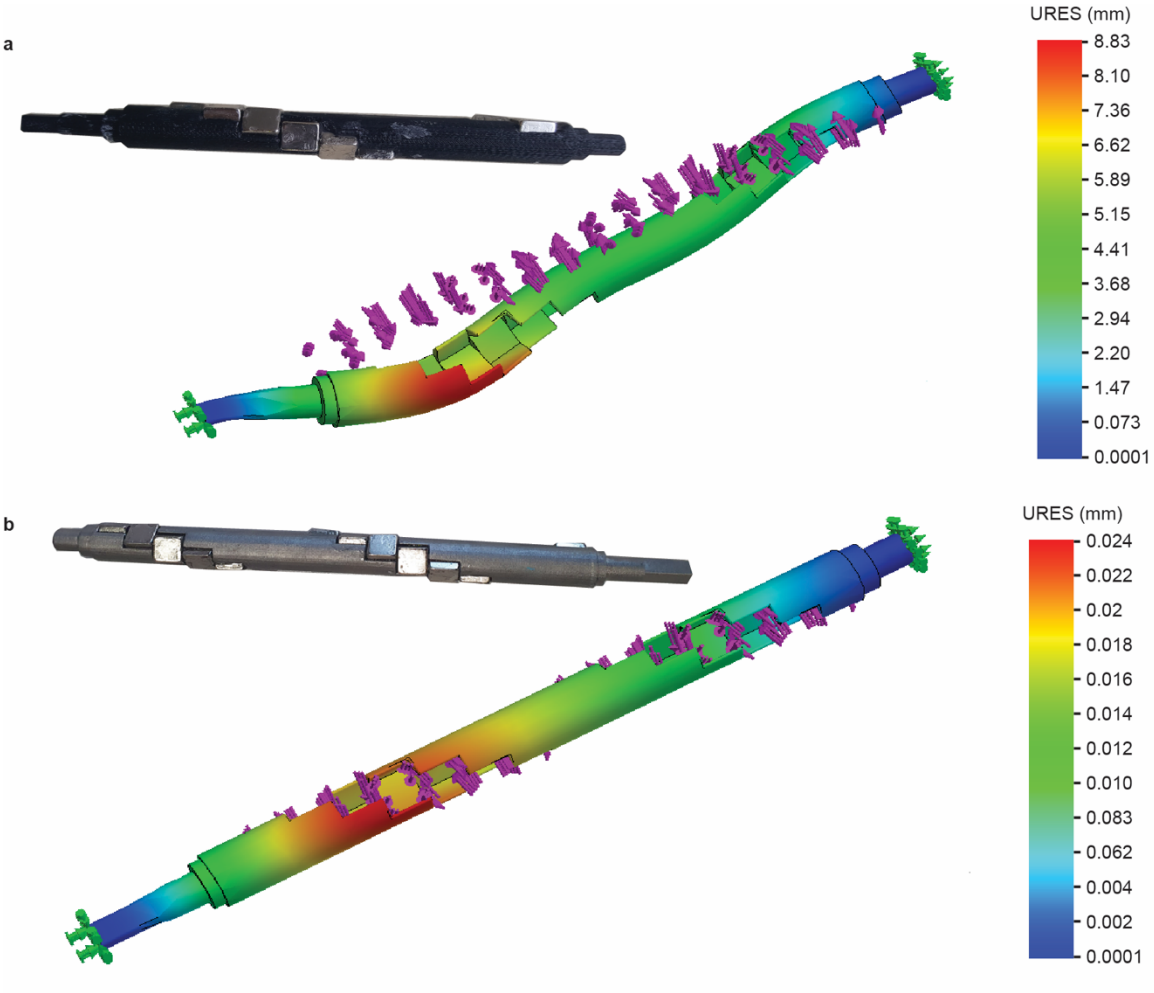

Fig. S6 | a, Deformation simulation with a printed ABS shaft. **b,** Deformation simulation with a printed shaft made of reinforced stainless-steel grade 316.

To rotate the three shafts according to the initial magnetic design, four spur gears and two worm gears were used (Fig. S7b). All shafts of the linear pump were made of metal using metal 3D printing (Fig. S8a). In addition, stainless steel with special properties for the shafts has been used for all shafts. All the axes responsible for the rotation of the spur gears were printed from durable aluminum (Fig. S8b). The magnets (cube-shaped NdFeB with dimensions of 10 mm) were inserted into the shaft with a strong glue (Fig. S8c). All main gears were made of special material in the intended size as specified in Table 1.

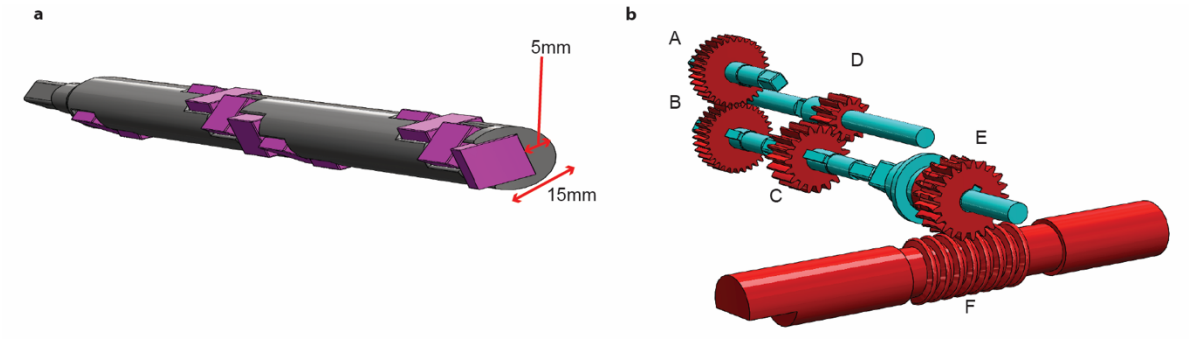

Fig. S7 | a, Cross section of the shaft, showing the free thickness of the shaft. **b,** Gears design arrangement.

Table 1. Gears mechanical specifications

Specification	**Gear**					
	A	B	C	D	E	F
Module	1	1	1.5	1.5	1.5	1.5
Number of Teeth	32	32	20	10	20	-
Surface Durability (Nm)	0.9	0.9	7.33	0.89	-	-
Pressure Angle (°)	20	20	20	20	20	20
Material	*(S45C)	*(S45C)	*(S45C)	*(S45C)	*CAC702 (AlBC2)	*SCM440
Tooth Finish	Cut	Cut	Ground	Cut	Cut	Ground
Bending Strength (Nm)	11.05	11.05	17.98	9.97	-	-
Weight (gr)	56	56	100	-	100	740

*(S45C): Carbon steel, CAC702 (AlBC2): Medium carbon chromium-molybdenum alloy steel, SCM440: Medium carbon chromium molybdenum alloy steel

Fig. S8 | a, Pump axles (including the axles on which the magnets are installed, as well as the axles responsible for the maintenance and rotation of the gears. **b,** Assembling axles with pump spur gears. **c,** Installing 16 cubic magnets on the shaft. **d,** Worm gears

2.2 Simulation of wheel worm gear

To check the characteristics and resistance of the wheel worm gear inside the gearbox, its simulation (Fig. S9) was done with the over-design value for torque (1000 N.m). This simulation was done to predict the resultant displacement (URES), stress, and safety factor (FOS) for worm gear to transmit power to the whole system.

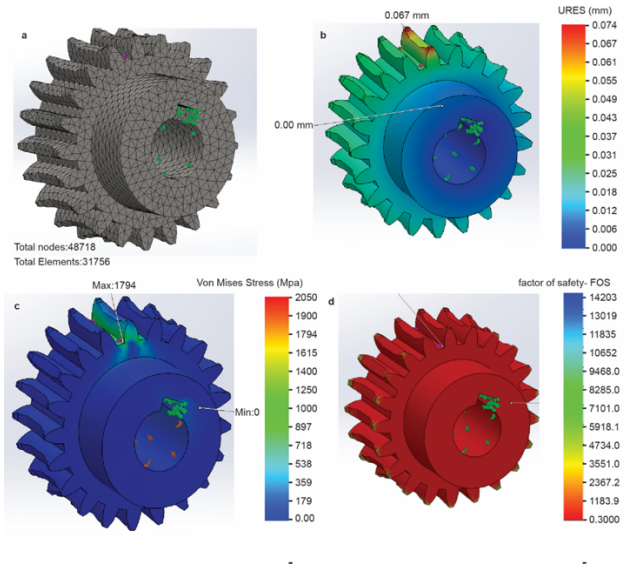

Fig. S9 |a, Solid mesh with a maximum element size of 1.5 mm. **b,** Resultant Displacement values under the maximum force on the gear. **c,** von mises stress changes in the pressure points in the gear. In fact, it is a quantity that describes the magnitude of forces that cause deformation. Stress is defined as force per unit area. **d,** Factor of safety values according to gear material.

2.3 Assembling the linear pump QL

First, the main components were designed and placed (Fig. S10). The assembly of the main body of the linear pump was done in four steps. After designing and fabricating the rotating parts from resistant metals (such as shafts and axles), the main body was printed with ABS polymer. First, according to the design of the linear pump driving force, the main body of the pump was designed and then printed with 3D printer technology using ABS polymer (Fig. S11). Then, the shafts and two spur gears (A) and (B) were attached (Fig. S12a). The main gears were attached to each other with a clearance of 0.1 mm. In the next step, the spur gears (D) and (C) were also installed in the pump (Fig. S12b). Then the worm gears and their accessories were connected to the system (Fig. S12c) and finally the gear system was installed on the electromotor (Fig. S12d).

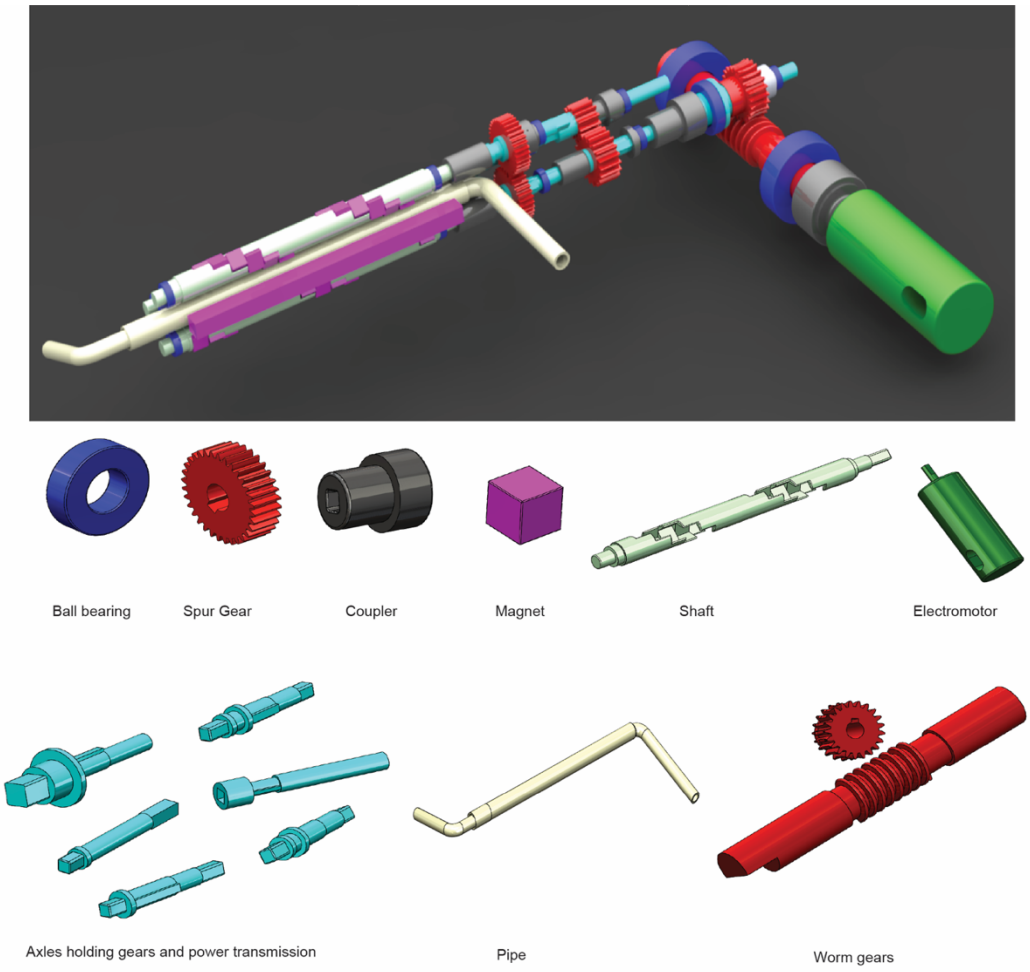

Fig. S10 | The design and positioning of the linear **QL** pump.

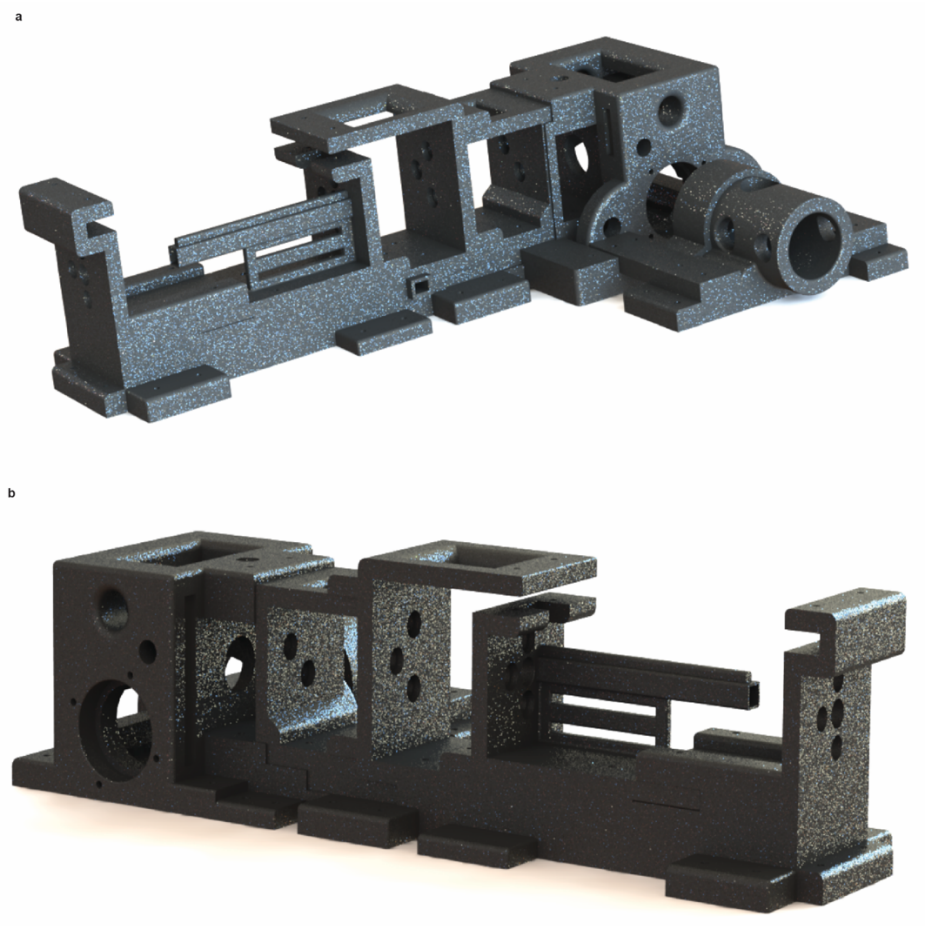

Fig. S11 | The main body of the linear pump **QL**. **a,** Front view. **b,** back view

Fig. S12 | a, Positioning the shafts in the pump and adding two spur gears. **b,** Adding a spur gear for the shaft with twice the speed of the other shafts. **c,** Positioning of the central power axis system of the pump. **d,** Positioning of the gearbox in the electromotor.

2.4 Pattern of moving ferrofluid in linear pump

The spiral rotation of the ferrofluid inside the tube in a certain period of time creates a negative pressure inside the tube, which provides the liquid transfer (Fig. S13). The spiral motion of the fluid is caused by the intended movement of the shafts.

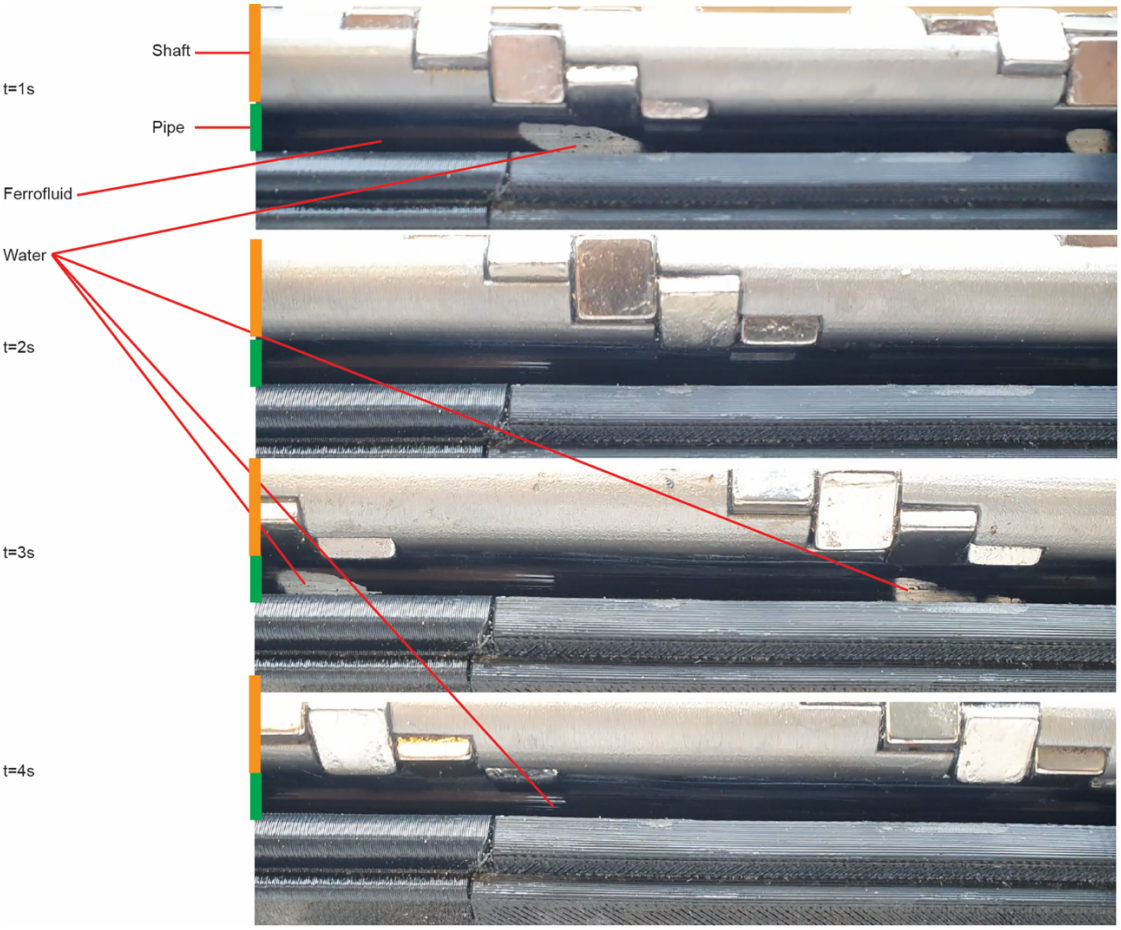

Fig. S13 | Showing the spiral movement of ferrofluid and its rotation in a period of 4 seconds.

3. Pump performance curves

The magnetic pump produces rotation in the rotating disc by the rotation of the electric motor, and the energy of the electromagnetic force increases the internal energy of the ferrofluid particles and causes them to move and circulate the fluid in the pump. Therefore, for each flow value, there is a pressure value that the pump must overcome. However, for magnetic pumps, the pressure decreases as the flow rate increases. Therefore, the results of the hydrodynamic characteristics and efficiency of the **QR3** at 110 rpm show that the best efficiency point (BEP) is about 700 mL min^{-1} (Fig. S14a). The shut-off head is the total head that the pump can deliver at zero flow. In comparison, the **QR2** pump (Fig. S14b) performed best at a flow rate of about 150 mL min^{-1} at the same speed, and the BEP for the **QR1** (Fig. 7c) and linear pump (Fig. S14d) was achieved at flow rates of 9 mL min^{-1} and 5 mL min^{-1}, respectively.

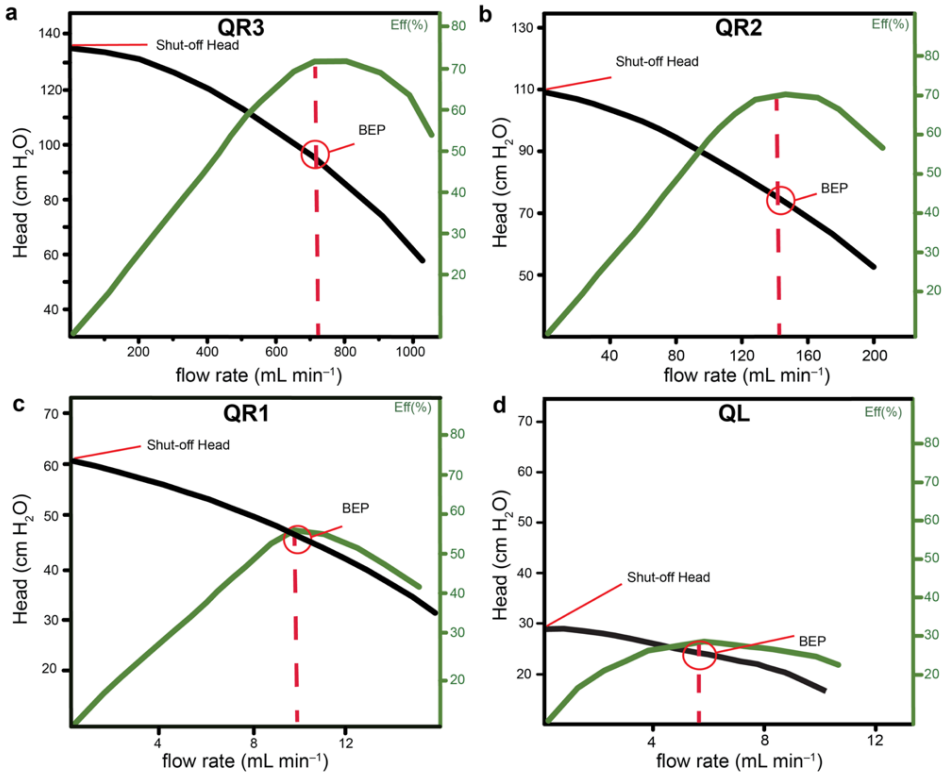

Fig. S14 | Pump curves for: a, rotary pump **QR3**. **b,** rotary pump **QR2**. **c,** rotary pump **QR1**. **d,** linear pump **QL**.

4. The ECMO circuit

4.1 Circuit setup and oxygenator (1000 mL min^{-1})

Four ECMO circuits with four different pumps were studied separately (n = 3 for each configuration). The Chalice Medical ECLS (Extracorporeal Life Support) base tube package—in clinical use at the Nouvel Hôpital Civil of Strasbourg was used in all circuits. Components of the tubing package included 3/8" PVC (Polyvinyl chloride) tubing without surface treatment (Eurosets) and connectors. The oxygenator was connected to these pumps via 3/8" tubing. The experiments were performed over 48 hours. In all experiments (total blood volume in the circuit, 450 ± 45 mL), the temperature was kept constant at 37 ± 1 °C using water with a temperature of 40 °C (heat exchanger inlet) and a flow rate of 4 L min^{-1} . In all tests, the pressure (Honeywell, pressure sensor, 15 psi Max Overload 30 psi, Through Hole, 8 Pin PDIP) was measured before and after the oxygenator. The ECMO experiments were performed with a flow rate of 1±0.1 L min^{-1} , which is in accordance with pediatric implementations.

The flow rate for ECMO cycles was verified to be 1 L min^{-1} using the ultrasonic flow meter (Sonotec, CO.55/060SD V2.0). A specialized piping system was designed to remove air from the system (see below). Phosphate-buffered saline (PBS, Life Technologies SAS) was circulated for 20 min. Subsequently, by flowing blood and taking advantage of the density difference between blood and PBS, all the PBS was displaced from the circuit. Fresh, air -free blood was then able to circulate through the system. 16 All PBS was drained before blood transfusion, and air bubbles were removed from the circuits before the start of the tests so that there was no contact between air and blood during the tests. Purge gas (1.41 L min^{-1}), a mixture of oxygen, medical air, and carbon dioxide (5% CO_2 , 21% O_2 , and 74% N_2), was used in the experiments. The pH of the circuit was kept within the range of 7.35-7.45 by regulating the sweep gas and adding sodium bicarbonate. In every experiment, three samples were obtained: one before the start of the experiment, another after two hours of cycle operation, and a third 48 hours after the cycle operation. Plasma Free Hemoglobin (PFH) analysis was performed immediately after obtaining each sample, while von Willebrand factor (VWF) analysis was conducted on platelet-poor plasma (PPP) samples that were frozen at –30 °C.

Oxygenator. In the present study, we used a hollow membrane oxygenator made of polypropylene (PP) material (Quadrox-I by Maquet, a subsidiary of Getinge Group). The membrane oxygenator in the Quadrox-I eliminates carbon dioxide and infuses oxygen into the blood, which is then returned to the patient's circulatory system. The oxygenator has a surface area of 1.3 m^2, a filling volume of 175 mL, and does not have an integrated arterial filter, but it uses a standard 3/8" connection. Furthermore, this oxygenator can support flow rates ranging from 0.5 to 5 L min^{-1}.

Pressure meter. In all tests, the pressure (Honeywell, pressure sensor Honeywell, pressure sensor, 15 psi Max Overload 30 psi, Through Hole, 8 Pin PDIP) was measured before and after the oxygenator. An essential ECMO cycle characteristic that can reveal oxygenator blockage is oxygenator pressure drop.

4.2 Elimination of air from the circuit

To remove air from the system, the circuit was initially filled with phosphate buffered saline (PBS) (Fig. S15). During this stage, valves V_7, V_2, and V_4 should be opened, while valves V_6, V_5, V_3, V_1, and V_8 must remain closed. According to Stevin's law - also known as the law of communicating vessels - after a period of time (approximately five minutes), the levels of both tanks (D_1 and D_2) will equalize.

At this stage, the cycle contains numerous bubbles. To remove these bubbles from the system, valves V_6, V_2 and V_4 must be opened, and the other valves should remain closed. By using this valve design, PBS is pumped in and out of reservoir D_1 so that it functions as a gas-liquid separator, enabling the air to be released from the top of the system and expelled outdoors (Fig. S15b). Afterward, blood from reservoir D_3 is introduced into the system and PBS solution is discharged through valve V_3 (see panel c).

At this stage, valves V_4, V_6, V_7, V_1, and V_8 should be closed, while valves V_5, V_3, and V_2 should be regulated carefully to allow for effective blood displacement with PBS (Fig. S15d).

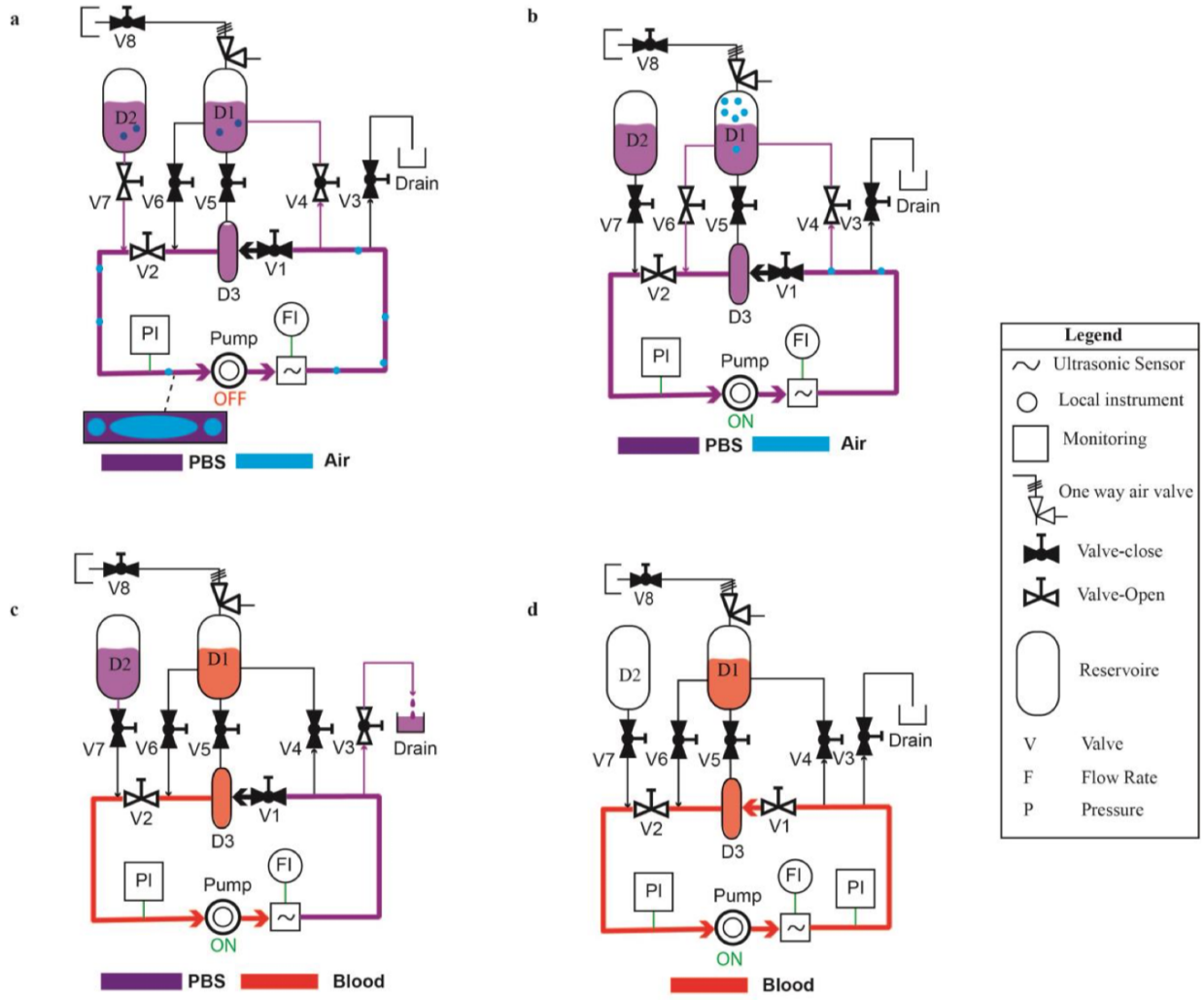

Fig. S15 | Removing air from the circuit. a) The pump is off initially and a 5 minutes equilibration is observed. b) The pump is turned on and the bubbles go to the tank and are discharged from the system. c) PBS is replaced with blood. d) Blood completely replaces PBS.

4.3 Pressure in the circuit

During the ECMO operation, the pressure was measured and monitored (Fig. S16a) at three different points according to the intended setup (Fig. S16b).

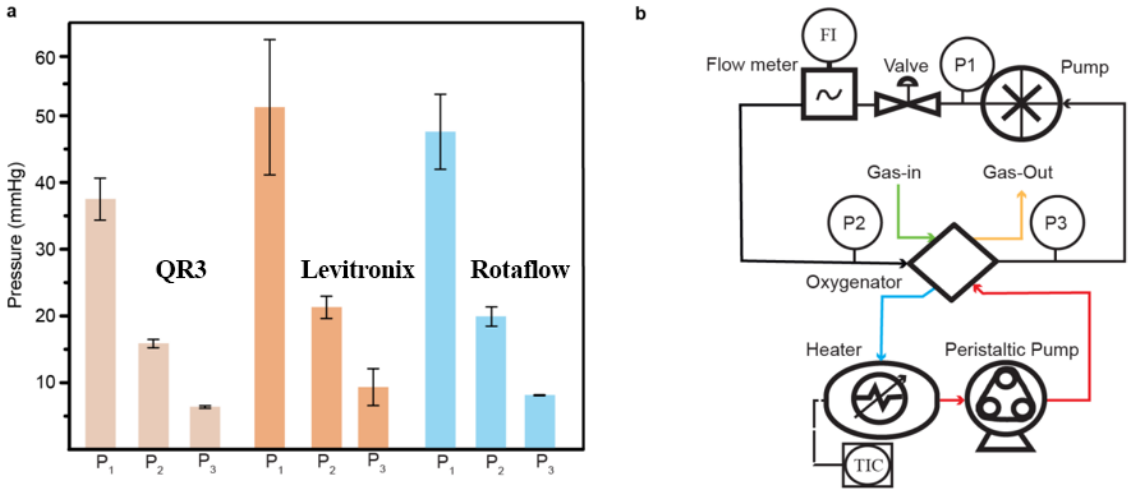

Fig. S16 | a, The average operating pressure of the ECMO cycle during 48 hours at 1000 mL min^{-1} with oxygenator in three regions: Inlet pressure (P1), pre-oxygenator pressure (P2), and post-oxygenator pressure (P3). **b,** Operating equipment of the ECMO system including pump, oxygenator, flow meter, pressure gauge, peristaltic pump, and heater.

4.4 Smaller circuits (4 & 150 mL min^{-1}, QL and QR1–2 pumps)

Pumping experiments without oxygenator were performed by submerging parts of the tubing in a hot water bath as to keep the blood temperature to 37 ± 1 °C.

4.5 NIH values

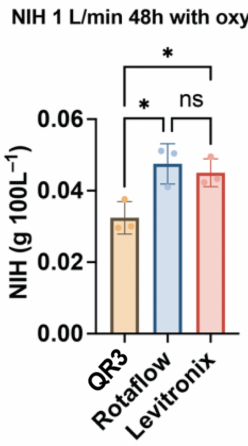

	ΔfHb (mg/dL)	V (mL)	Ht (%)	Q (L/min)	T (min)	NIH
QR3	397.29	400	31.8	1	2880	0.037632192
	350.3	400	38.3	1	2880	0.030018764
	320.8	400	33.5	1	2880	0.029629444
Rotaflow	597.1	400	38.4	1	2880	0.051085222
	480.02	400	38.5	1	2880	0.041001708
	561.8	400	35.4	1	2880	0.050405944
Levitronix	470	400	35.2	1	2880	0.0423
	519	400	39.9	1	2880	0.043322083
	579	400	38.5	1	2880	0.04945625
Peristaltic	1042.3	400	32.5	1	2880	0.097715625
	1200	400	37.5	1	2880	0.104166667
	950	400	40.7	1	2880	0.078243056

5. Measurement of ferrofluid leaching into blood

5.1 Method

The ferrofluid contamination in the pumped blood was determined by wet digestion analysis.[1] First, 0.5 mL of whole blood was placed in a beaker. To this was added 3 mL of a freshly prepared mixture of concentrated nitric acid and hydrogen peroxide [HNO_3:H_2O_2] (2:1 v/v) and allowed to stand for 10 minutes. The flask was then covered with a watch glass and heated to 60-70°C for 2 hours. Then 2 mL of nitric acid and 1 mL of H_2O_2 were added to the digests while the mixture was heated to 80°C until a clear digested solution was obtained. This solution was then diluted with 0.1 mL of nitric acid and further diluted with 100 mL of distilled water. The amount of ferrofluid in the solution was then quantified by atomic absorption spectroscopy (AAS; Agilent Technologies 200 Series AA) using the emission wavelength of iron (248.3 nm).

5.2 Operational conditions

The ferrofluid released from the pressure part of the pumps was measured after two hours of operation in a closed circuit (Fig. S17). In these experiments, PBS was first circulated for 20 minutes. After draining, the blood was circulated. These data were obtained in the control period between 2 minutes after pump start and up to 2 hours in a closed circuit at the optimal flow rate (BEP).

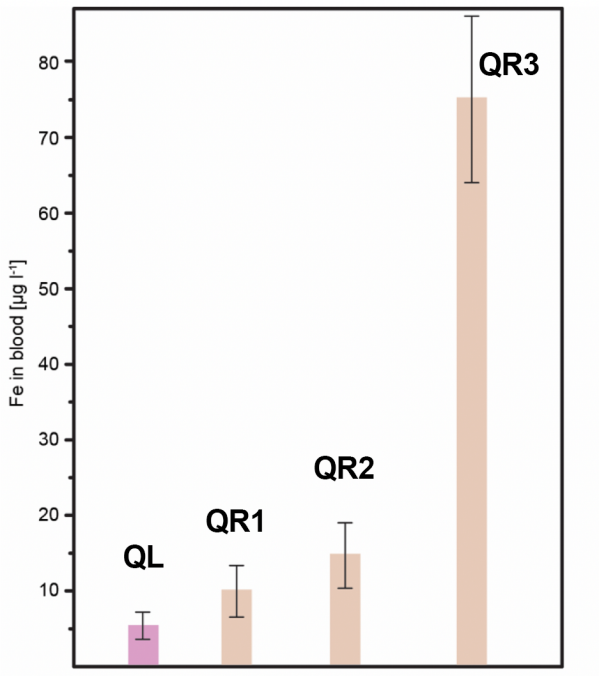

Fig. S17 | Comparison of total Fe detected in blood samples after two hours of closed loop pumping (without oxygenator).

6. Blood analysis

6.1 Blood preparation analysis

To obtain platelet-rich plasma (PRP) and platelet-poor plasma (PPP), each sample was centrifuged in a Sorvall RC3BP centrifuge. Whole blood was centrifuged at 250 revolutions per minute (rpm) for 16 minutes, and PRP was collected without brake. To produce PPP, a speed of 2500 rpm was maintained for 16 minutes. Platelet counting was performed using the Sysmex flagship analyzer, model XN 1000. Therefore, 200 µL PRP was counted in the instrument for each sample. PFH was calculated spectrophotometrically at specific wavelengths using ultraviolet-visible absorption (UV-Vis) of hemoglobin. For this purpose, the absorption spectrum of PRP was diluted 25-100 times with phosphate buffer after pumping the blood. Subsequently, the PFH concentration was estimated from the absorbance of PRP using the TECAN Infinite M Nano automata model.

6.2 VWF multimer analysis – gels

VWF multimer profile was performed essentially as follows. After circulation in the different pumps, plasma was diluted in sample buffer containing SDS and urea and loaded into 1% stacking high-gelling temperature agarose gel and 2-3% running agarose gels (50% high-gelling temperature agarose, SeaKem HGT Agarose, Lonza, Rockland, ME and 50% isoelectric focusing-agarose (GE Healthcare, Little Chalfont, United Kingdom). 20-hour gel electrophoresis was performed at 4°C, 57V and followed by 18-20h wet capillary transfer blotting on a methanol pre-activated PVDF membrane (Immobilon-P, Millipore Corporation, Billerica, MA). VWF was revealed with an in-house alkaline phosphatase-conjugated polyclonal goat anti-VWF and detected with a colorimetric alkaline phosphatase-substrate kit (Bio-Rad Laboratories, Hercules, USA). Membranes were imaged with a G: BOX Chemi XT16 Image Systems. The area of each gel band was analyzed using ImageJ and normalized (0–1).

6.3 VWF multimer analysis – ELISA

Total VWF. Microtiter wells coated with rabbit polyclonal anti-VWF antibodies (5 µg/mL; Dakocytomation, Glostrup Denmark) were incubated with plasma samples diluted in PBS/0.01% Tween-20/0.1% bovine serum albumin. Bound VWF was probed using peroxidase-labeled rabbit polyclonal anti-VWF antibodies (Dakocytomation, Glostrup Denmark) and detected via hydrolysis of 3,3‘,5,5‘tetramethylbenzidine. Normal pooled plasma was used a reference.

Intact VWF. Intact-VWF is referred to as VWF being recognized by nanobody KB-VWF-D3.1, which selectively binds to VWF that has not been degraded by ADAMTS13. Intact-VWF was measured as follows. Microtiter wells coated with KB-VWF-D3.1 (5 $\mu g\ mL^{-1}$) were incubated with plasma samples diluted in PBS/0.01% Tween-20/0.1% bovine serum albumin. Bound intact-VWF was probed using peroxidase-labeled rabbit polyclonal anti-VWF antibodies (Dakocytomation, Glostrup Denmark) and detected via hydrolysis of 3,3',5,5'-tetramethylbenzidine. Normal pooled plasma was used a reference. The relative content of intact-VWF was calculated by dividing the intact-VWF antigen concentration by the total VWF antigen concentration.

7. Platelets aggregation

7.1 Method

Light transmission aggregometry (LTA) was used to analyze platelet aggregation[2]. Aggregation was expressed as the maximum percentage change in light transmission from baseline. Three agonists including arachidonic acid (AA), adenosine diphosphate (ADP) and collagen were used. For the ADP assay, 30 µL of ADP at a concentration of 50 $\mu mol\ L^{-1}$ was added to 270 µL of PRP for a final concentration of 5 µM. For assay with AA in 294 µl of PRP, 6 µl of AA at a concentration of 0.05 $mol\ L^{-1}$was added for a final concentration of 1 mM. In the case of collagen, two different final concentrations of 2.5 $\mu g\ mL^{-1}$ and 1.25 $\mu g\ mL^{-1}$ were used (in 270 µL of PRP, we added 30 µl of collagen at 25 $\mu g\ mL^{-1}$, while in 285 µl of PRP, we added 15 µl of collagen at 25 $\mu g\ mL^{-1}$). Platelet aggregation was induced by addition of the agonist and recorded for 8 min on a 4-channel semi-automatic platelet aggregometer (APACT 4004). The response of each donor after pumping was compared to the control sample.

7.2 Operation

Platelet aggregation was performed for **QR3** over a period of 6 hours[3] and at a flow rate of 1L min^{-1} at a temperature of 37°C according to standard conditions[3] (Fig. S18). There is a 12.4% decrease between the maximal aggregation (%) of adenosine diphosphate (ADP) before versus after pumping. For collagen concentrations of 2.5 $\mu g\ mL^{-1}$, 1.25 $\mu g\ mL^{-1}$, and 1 mM arachidonic acid (AA), the decreases are about 2.5%, 3.5%, and 0.32%, respectively (see Fig. S18). The acceptable range for adenosine diphosphate (ADP) is between 60-100% (aggregation versus the non-pumped initial sample), for collagen concentrations of 2.5 µg mL^{-1} between 70-100%, for collagen concentrations of 1.25 $\mu g\ mL^{-1}$ is between 55-100%, and for arachidonic acid (AA) between 70-100%.* In fact, all aggregations values after pumping fall within the normal range established at the laboratory so the findings demonstrate that the **QR3** pump has no negative effects on the ability of platelets to aggregate.

* Internal document of l'Etablissement français du sang (EFS) : Tableau recapitulatif des intervalles de references utilises au laboratoire d'hemostase specialisee, 2023. ALC/LAB/HES/POA/FO/201

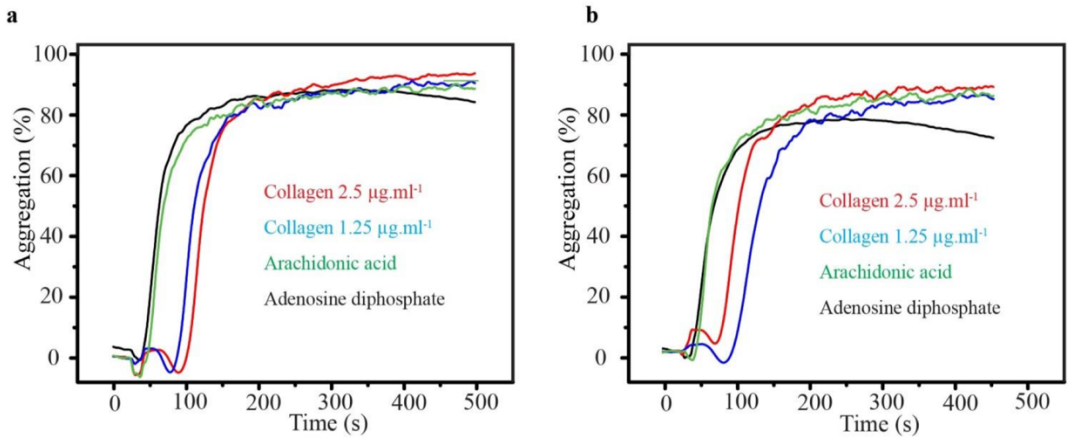

Fig. S18 | Platelet aggregation. a) control sample (without pumping), b) after 6 hours of pumping with **QR3** at 1L min^{-1} flowrate (without oxygenator).

Abbreviations

PFH, Plasma-free hemoglobin; AAS, atomic absorption spectroscopy; BEP, Best efficiency point; LTA, light transmission aggregometry; AA, arachidonic acid; ADP, adenosine diphosphate; PRP, Platelet-rich plasma; PPP, Platelet-poor plasma; RPM, Revolutions per minute.

8. References

1. Yahaya, M., Shehu, A. & Dabai, F. Efficiency of Extraction of Trace metals from Blood samples using Wet Digestion and Microwave Digestion Techniques. *J. Appl. Sci. Environ* **17(3)**, 365–369 (2013).
2. Harrison, P. *et al.* Guidelines for the laboratory investigation of heritable disorders of platelet function. *Br Haemotol* **155(1)**, 30–44 (2011).
3. Standard Practice for Assessment of Hemolysis in Continuous Flow Blood Pumps. in *AMERICAN SOCIETY FOR TESTING AND MATERIALS 100 Barr Harbor Dr., West Conshohocken, PA 19428 Reprinted from the Annual Book of ASTM Standards. Copyright AST* vol. 13.01 (1998).